



Research article

Electrical switching properties of Ag₂S/Cu₃P under light and heat excitation

Xin Guo, Yanfei Lv^{*}, Manru Chen, Junhua Xi, Li Fu, Shichao Zhao

College of Materials & Environmental Engineering, Hangzhou Dianzi University, Hangzhou, 310018, China

ARTICLE INFO

Keywords:

Electrical switching
Silver sulfide
Copper phosphide
Heterostructure
Photovoltaic effect
Thermoelectric effect

ABSTRACT

In this paper, we prepared and investigated the electrical switching behaviors of Cu₃P/Ag₂S heterojunction in the absence/presence of light/heat excitation. The structure exhibited bipolar memristor characteristics. The resistive switching mechanism is due to the formation of Ag conductive filaments and phase transition in Cu₃P. We found that the resistance ratio (R_{OFF}/R_{ON}) increased by a factor of 1.4/1.8 after light/heat excitation. The underlying mechanism was due to the photoelectric effect/Seebeck effect. Our results are helpful for the understanding of the resistive switching performance of Cu₃P/Ag₂S junctions, providing valuable insights into the factors influencing resistive switching performance and a clue for the enhancement of the memristor performance.

1. Introduction

Memristor, a type of resistive switching device capable of retaining their resistance states even after the power is turned off, has obtained significant attention due to their promising applications in information storage, intelligent computing system design, neural networks and other emerging technologies [1–5]. Silver sulfide (Ag₂S), with combined electronic and ionic transport properties, is one of the earliest materials studied for memristor. The conduction filament theory was initially proposed to understand the memristive behavior of Ag₂S. As the investigation into memristor progressed, researchers discovered that multi-layer structures exhibited significantly improved electrical switching properties compared to single layer. For instance, Saika et al. found that an Ag₂S/oxidized graphene structure preserved both the switching properties of Ag₂S and tunneling currents modulated by oxidized graphene. Furthermore, this structure displayed notable volatility-based neuromorphic properties [6]. Recently, multi-layer structures based on p-type and n-type semiconductor materials have attracted lot of attentions [7–9]. The rectification effect caused by p-n diode results in a significantly reduction of power consumption, as well as a decrease in the sneak-path current between memristor crossbar arrays [10–12].

In conjunction with the investigation of multilayers, the influence of external excitations on memristor behaviors has come under study. For example, Mou, N. I. et al. Investigated the effect of light irradiation on the Ag₂S resistive switching properties. They observed that the switching time and turn-off voltages were reduced after illumination, which can be attributed to changes in sulfur valency and photo-induced alterations in oxidation/reduction potential [13].

Copper phosphide (Cu₃P), a p-type material, has been studied for its resistive switching performances by few groups [14,15]. In our previous work, we reported that Cu₃P memristor exhibited a high On/Off ratio (2.1×10^4), high work frequency (approximately 5000

^{*} Corresponding author.

E-mail addresses: lvyanfei@hdu.edu.cn (Y. Lv), zhaoshichao@hdu.edu.cn (S. Zhao).

Hz), high stability (endurance 2×10^3 , retention time larger than that 2×10^4) and low switching voltage (less than 0.35 V) [15]. However, the memristor behavior of $\text{Ag}_2\text{S}/\text{Cu}_3\text{P}$ double layer structures remains unclear, as does the influence of the external effects such as light irradiation and thermal excitation on the memristor behavior. In this study, we first prepared Ag_2S thick films and further combined them with Cu_3P thick film to form $\text{Ag}_2\text{S}/\text{Cu}_3\text{P}$ stacked structures. Then, we investigated the effect of visible light illumination and asymmetric heating of electrodes on the resistive switching properties of the structure. The structure exhibited bipolar switching behaviors. The underlying mechanism was due to the formation of metal conductive filaments in Ag_2S and phase transition in Cu_3P . We found that these excitations affected the resistance of the structure. The On/Off ratio increased after light and heat excitation, attributable to the photoelectric effect and Seebeck effect, respectively. In this paper, we demonstrated for the first time that the Seebeck effect influences resistive switching behaviors, and its effect is larger than that of the photoelectric effect. Our results contribute to the understanding of resistive phenomena in multilayers under light and heat excitation.

2. Experimental

2.1. Preparation of Ag_2S thick film

We utilized the ductile property of Ag_2S to prepare flexible thick films by grinding Ag_2S powders, as shown in Fig. 1a [16,17]. A certain amount of Ag_2S particles (0.5 g) were placed into an agate grinding bowl. The particles were then ground at a speed of 150 rpm with a mechanical pressure of approximately 100 N for 20 min.

2.2. Preparation of Cu_3P thick film

Copper phosphide was prepared using the phosphorization method, as shown in Fig. 1b [18]. Sodium hypophosphite (NaH_2PO_2 , 0.5 g) and copper foil sealed in a glass tube were heated to 300°C and kept for 30 min under inert gas protection. Afterward, the tube was naturally cooled to room temperature to obtain Cu_3P on the copper substrate. Then the Cu_3P bulk film was obtained by mechanically separation from the substrate. (Note, the residual gases in the tube should be removed by vacuum pumping and purified with a copper sulfide solution before removing the sample).

2.3. Preparation of $\text{Ag}_2\text{S}/\text{Cu}_3\text{P}$ structure

The $\text{Ag}_2\text{S}/\text{Cu}_3\text{P}$ junction was prepared by stacking a Ag_2S bulk film on a Cu_3P thick film, as shown in Fig. 1c. Ag_2S and Cu_3P films were squeezed together by the pressure of the test probes. Two Au tips used as electrodes were connected with the Ag_2S and Cu_3P , respectively. The tip diameter is approximately $150\ \mu\text{m}$. The distance between the two tips is approximately $500\ \mu\text{m}$ controlled by a spiral micrometer under the help of an optical microscope.

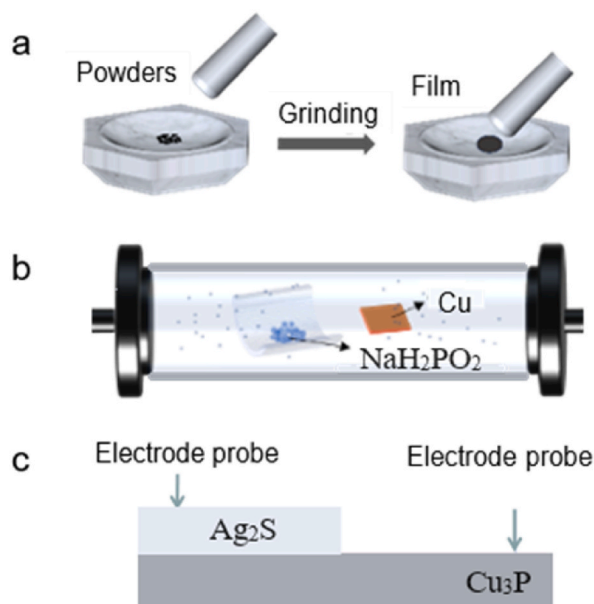


Fig. 1. Schematic diagrams of the preparation process of Ag_2S film (a), Cu_3P film (b), and $\text{Ag}_2\text{S}/\text{Cu}_3\text{P}$ device structure (c).

2.4. Characterizations

The crystal structures were characterized using an X-ray diffractometer (XRD, Thermo ARLXTRA). The surface morphology, microstructure, and elemental composition of the samples were analyzed using a scanning electron microscope (SEM, FEI Apero S, model SU-1050). The conduction type of Ag_2S and Cu_3P was tested by hot-probe methods. The electrical properties were conducted on an electrochemical workstation (Shanghai Chenhua CHI760E). The reference electrode (white) and counter electrode (red) were connected to the Cu_3P electrode, while the working electrode (green) was connected to Ag_2S . The probe electrodes were applied to the device surface by gravity. CV mode was selected to test the current-voltage curve (I - V curve). The voltage scanning rate was 0.05 V/s, the voltage acquisition interval was 0.001 V. In the thermal excitation experiment, the electrode connected to silver sulfide was heated by a heater, and the electrode temperature was measured by a thermocouple. In the study of the effect of light excitation on the electrical properties, the 365 nm ultraviolet light with a power density of 10 W/cm^2 was used. The photon energy of the UV light is greater than the band gap of Ag_2S and Cu_3P to produce photoelectrons.

3. Results and discussion

3.1. XRD and SEM

Fig. 2a shows the XRD pattern of the bulk silver sulfide (Ag_2S) film prepared with different grinding times. All discernible peaks correspond to Ag_2S . The Ag_2S powder before grinding (0 min, black color) exhibited a polycrystalline structure without preferred crystal orientation. After grinding 20 min (red color), a tendency of growth along the (-104) crystal plane orientation emerged. Fig. 2b and c shows the SEM image and EDX spectra of Ag_2S , respectively. From Fig. 2b, it can be observed that the silver sulfide films were dense and continuous. The striped patterns are due to grinding marks. From Fig. 2c, it can be seen that the samples consisted of silver (Ag, 75.9 %, atomic) and sulfur (S, 23.0 %), indicating that the silver sulfide was not oxidized during the grinding process. The presence of approximately 1.0 % oxygen in Fig. 2c is due to measurement errors or carbon dioxide absorption.

3.2. Electrical switching of $\text{Ag}_2\text{S}/\text{Cu}_3\text{P}$

Fig. 3a shows representative I - V curves of the $\text{Ag}_2\text{S}/\text{Cu}_3\text{P}$ structure. We observed that as the voltage sweeps ($0 \text{ V} \rightarrow 0.2 \text{ V} \rightarrow 0 \text{ V}$), the device undergoes a transition from a high resistance state (HRS) to a low resistance state (LRS). During the voltage sweeping ($0 \text{ V} \rightarrow -0.2 \text{ V} \rightarrow 0 \text{ V}$), the device recovers from LRS to the initial HRS. Therefore, the structure exhibits bipolar memristor characteristics. The resistive state transition mechanism is related to the formation of Ag metal conductive filaments in Ag_2S and phase change in Cu_3P [15, 19]. For the latter, the alternation of phosphorus formation by oxidizing phosphorus anions and subsequent phosphorus reduction results in state switching. The area of switching window does not decrease after 16 circles, indicating that the structure is stable. Fig. 3b presents the variation of resistance in HRS and LRS with the number of cycles. The resistance of HRS slowly increases with the rise of cycle number, while LRS fluctuates around $(6 \pm 1) \text{ M}\Omega$. Fig. 3c shows the corresponding bar chart of the switch ratio ($R_{\text{OFF}}/R_{\text{ON}}$), in which R_{OFF} and R_{ON} represent the resistance of HRS and LRS, respectively. The $R_{\text{OFF}}/R_{\text{ON}}$ remains relatively constant with a value of 1.3. Fig. 3d displays the first cycle I - V curve in a double logarithmic coordinate system within the positive voltage scanning range. Through linear fitting, the slope corresponding to the linear part of LRS is determined to be 1.12, indicating that the carrier transport mechanism in LRS follows Ohm's law, in which the current (I) is proportional to the voltage (V) [15]. In contrast, the slopes of the linear part of HRS in the high voltage region are 0.85, 1.30, and 1.16, indicating Ohmic transport of carriers [13]. While, in the low voltage region, the slope is 0.27, consistent with the Schottky law, in which $\ln(I)$ is proportional to $V^{0.5}$ [15]. The Schottky rectifying effect is caused by the pn junction space charge field formed at the $\text{Ag}_2\text{S}/\text{Cu}_3\text{P}$ interface. The conduction type of n- Ag_2S and p- Cu_3P was proved by hot-probe method [20,21].

Furthermore, Fig. 3e shows that within the negative voltage scanning range, LRS satisfies Ohm's law (slope of 0.96), while the carrier transport in the HRS, in addition to following Ohm's law, also follows Child's law (slope of 1.76) in the high voltage region [15].

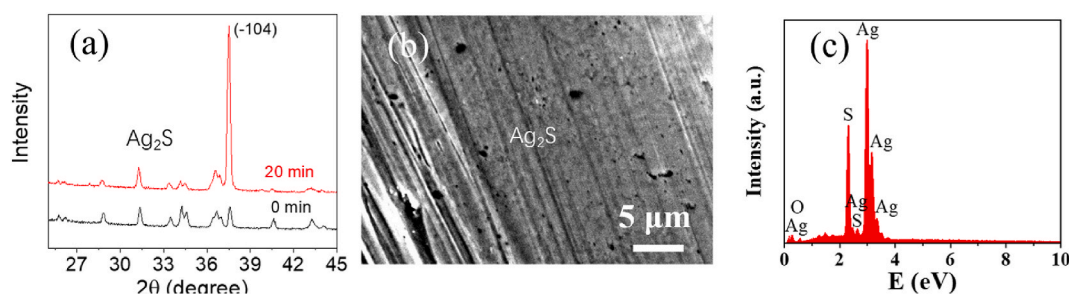


Fig. 2. (a) XRD patterns of silver sulfide before (0 min, black color) and after grinding (20 min, red color). SEM image (b) and EDX (c) of silver sulfide after 20 min of grinding. The scale bar in (b) is $5 \mu\text{m}$. (For interpretation of the references to color in this figure legend, the reader is referred to the Web version of this article.)

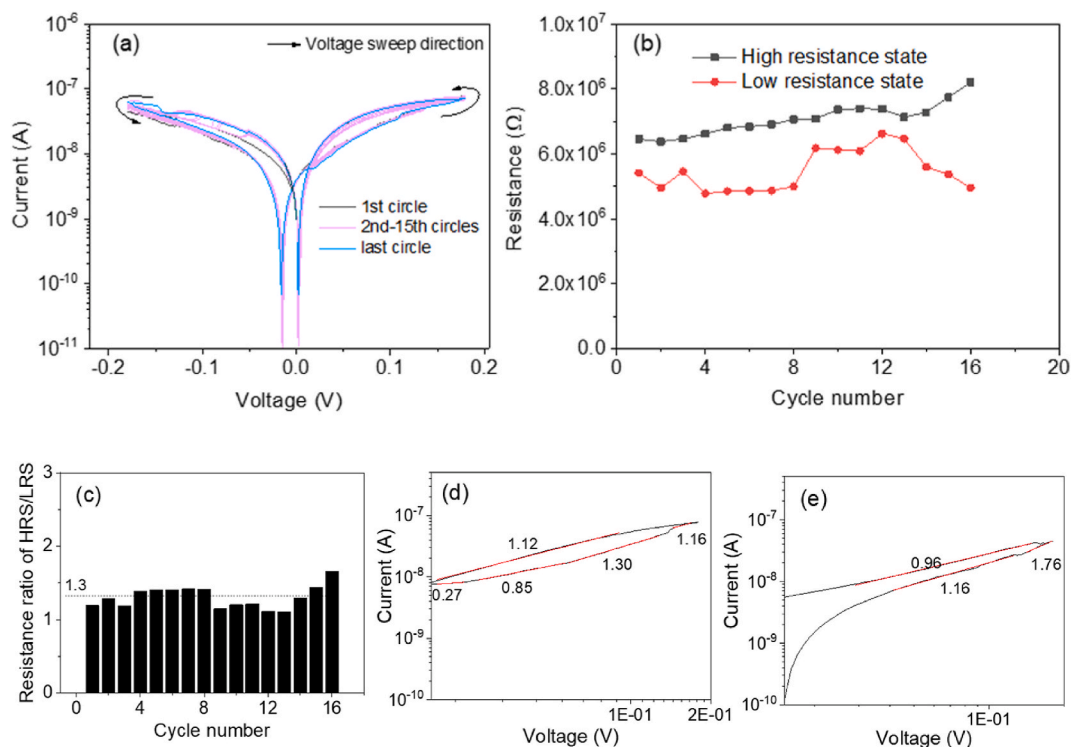


Fig. 3. I-V curves, endurance, off/on ratio of Ag₂S/Cu₃P structure. (a) Typical 16 cycles of I-V curves at room temperature. (b) Variation of resistance of high resistive state (HRS) and the low resistive state (LRS) with the number of test cycles. The values correspond to a voltage of 0.050 V in (a). (c) Resistance ratio between the HRS and LRS (R_{OFF}/R_{ON}). I-V curve of the first circle in logarithmic coordinates for the positive (d) and negative (e) bias voltage regions, respectively.

These experimental results indicate that the Ag₂S/Cu₃P device exhibits resistive switching performance, and the carrier transport mechanisms differ in different resistance states.

3.3. Effect of light excitation on the electrical switching of Ag₂S/Cu₃P

Fig. 4 shows the I-V curves of the Ag₂S/Cu₃P structure before and after light excitation. The resistance of both HRS and LRS decreases exponentially with the number of cycles, with a decay time constant of (2.6 ± 0.2) s (Fig. 4a and b), which is due to the photogenerated current [22]. The intersection point of the I-V curves moves towards negative voltage after irradiation, which is due to the photovoltaic effect [23]. Fig. 4c displays the relationship between the R_{OFF}/R_{ON} and the number of test cycles. We observed that the value of R_{OFF}/R_{ON} after illumination remains relatively stable at (1.8 ± 0.2) , which is larger than the value of 1.3 (Fig. 3c) obtained in dark. Consequently, illumination enhances the R_{OFF}/R_{ON} ratio of the structure by 1.4 times compared to the dark condition. This enhancement is attributed to the photoelectric effect, which increases the carrier concentration [24]. In the positive voltage region (Fig. 4d), LRS follows Schottky law, with slopes ranging from 0.13 to 0.53; while HRS in the high/low voltage region follows Ohm's law/Schottky law (slope: 0.83/0.18) [15]. In the negative voltage region (Fig. 4e), LRS follows Ohm's law (slope 1.35); HRS follows Schottky law/Child's law in the low/high voltage region [15]. Therefore, the carrier transport mechanism of the LRS/HRS in the positive/negative voltage region changes after light irradiation.

3.4. Effect of asymmetric heating on the electrical switching of Ag₂S/Cu₃P

Fig. 5a shows the I-V curves of the Ag₂S/Cu₃P structure with Ag₂S layer being heated. The cross point of the figure-8 shape deviates towards positive voltage, which is due to the Seebeck effect [25]. The resistances both of HRS and LRS decrease with the rise of temperature (Fig. 5b), which is possibly due to the increased ion diffusion rate. The initial R_{OFF}/R_{ON} is 1.3. With the increase of temperature, R_{OFF}/R_{ON} first increases slowly, then increases exponentially, and finally tends to stabilize (with an average value of 2.3) in Fig. 5c. The reason for the stabilization of R_{OFF}/R_{ON} is due to the stable temperature difference formation between silver sulfide and copper phosphide.

The final R_{OFF}/R_{ON} of the structure heated at about 100 °C is 1.8 times that at room temperature. We speculated that this phenomenon arises from the Seebeck effect, wherein the thermoelectric voltage partially offsets the external electric field, resulting in a substantial decrease in R_{ON} . The carrier transport of LRS in the high positive region follows the Schottky law (slope 0.58) (Fig. 5d),

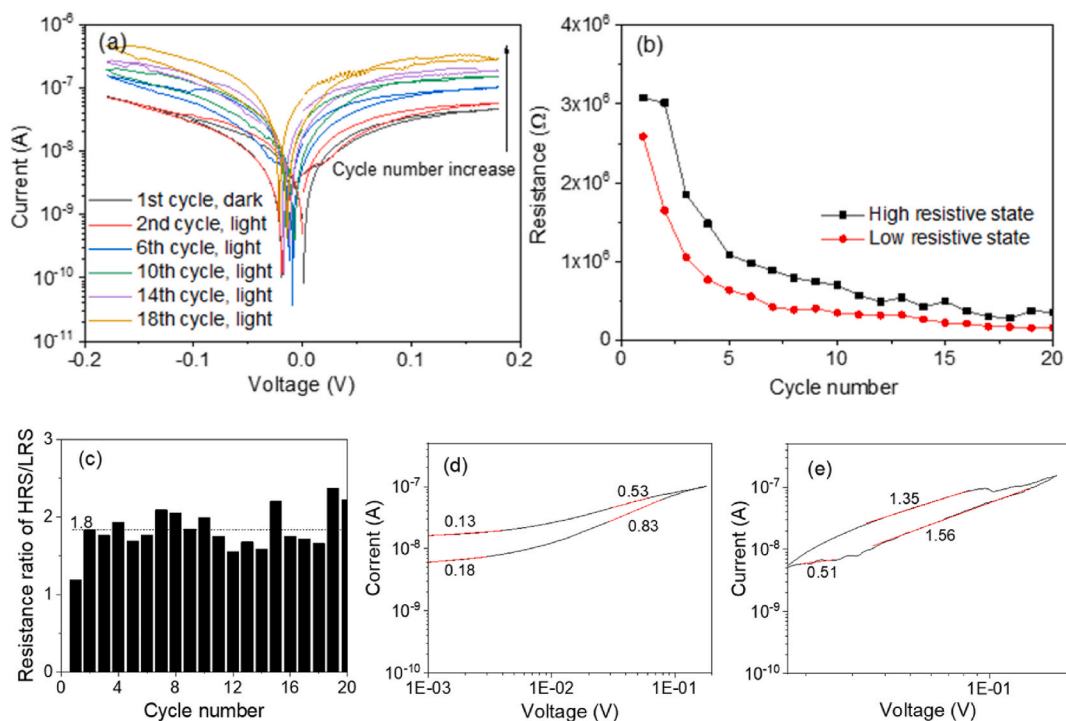


Fig. 4. Electrical switching performance of Ag₂S/Cu₃P structure under light irradiation. (a) Representative cycles of I–V curves. (b) Variation of resistance of HRS and LRS with the number of test cycles. The values correspond to a voltage of 0.020 V in (a). (c) Resistance ratio between the HRS and LRS (R_{OFF}/R_{ON}). I–V curve of the 6th circle in logarithmic coordinates for the positive (d) and negative (e) bias voltage regions, respectively. The first I–V curve was obtained under dark, while others were under light. The excitation light wavelength is 365 nm.

while in the low voltage region follows Child's law (slope 1.58) [15]. For HRS, the slope is in the range of from 0.28 to 1.42, indicating that the carrier transport follows the space charge limited current (SCLC) law [15]. In the negative voltage scan range (Fig. 4e), for LRS, the slope in the linear region ranges from 0.62 to 0.76, which basically follows the Schottky law; while for HRS, the slope in the linear region ranges from 1.11 to 1.60, which is consistent with the Ohm's law and Child's law, respectively [15]. The carrier transport mechanisms are different before and after light/heat excitation.

4. Conclusions

In this study, we prepared and studied the electrical switching properties of Ag₂S/Cu₃P structure before and after light/thermal excitation. The structure exhibited stable bipolar switching properties. The resistance switching mechanism was attributed to the formation of Ag metal filaments and phase change in Cu₃P. The effects of illumination and heat on the resistive switching properties were investigated. We found that the resistance of device decreased after light irradiation and heating, which was due to the photovoltaic effect and Seebeck effect, respectively. In addition, we found that both light illumination and heating can enhance the switching ratio of R_{OFF}/R_{ON} . It increased by a factor of 1.4 and 1.8 after light illumination and heating, respectively. The effect of heating on the R_{OFF}/R_{ON} ratio is larger than that of light irradiation. The structure showed different carrier transport mechanisms in the absence/presence of light/thermal excitation. Our results are benefit for the understanding of the impact of photoelectric and thermoelectric effects on the memristor performance.

Data availability statement

Data will be made available on request.

CRediT authorship contribution statement

Xin Guo: Writing – original draft, Visualization, Investigation. **Yanfei Lv:** Methodology, Conceptualization. **Manru Chen:** Investigation. **Junhua Xi:** Investigation. **Li Fu:** Formal analysis. **Shichao Zhao:** Writing – review & editing, Conceptualization.

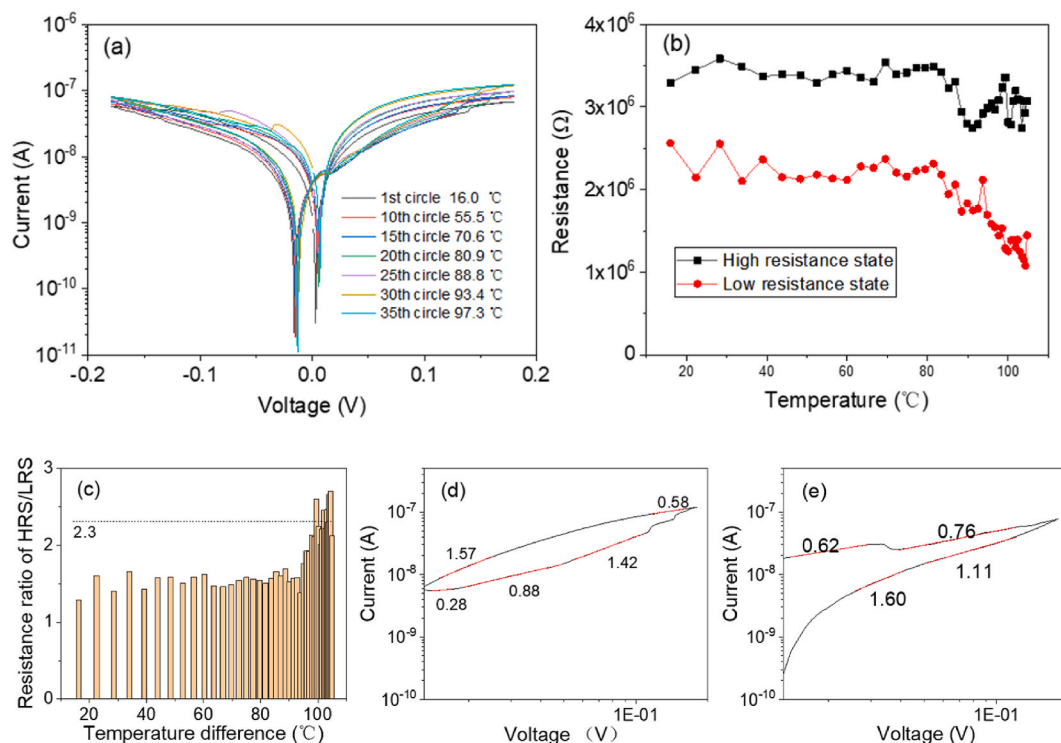


Fig. 5. Electrical switching performance of Ag₂S/Cu₃P structure under different temperature. (a) Representative I–V curves corresponding to different temperature. (b) Variation of HRS and LRS resistances with the number of test cycles at a voltage of 20 mV. (c) Switching ratio of HRS/LRS (R_{OFF}/R_{ON}) corresponding to different numbers of test cycles. (d) and (e) represent the double-logarithmic I–V curves for the 30th cycle under positive and negative voltages, respectively.

Declaration of competing interest

The authors declare that they have no known competing financial interests or personal relationships that could have appeared to influence the work reported in this paper.

Acknowledgements

Not applicable.

References

- [1] S. Pi, C. Li, H. Jiang, W.W. Xia, H.L. Xin, J.J. Yang, Q.F. Xia, Memristor crossbar arrays with 6-nm half-pitch and 2-nm critical dimension, *Nat. Nanotechnol.* 14 (1) (2019) 35–39.
- [2] I. Boybat, M. Le Gallo, S.R. Nandakumar, T. Moraitis, T. Parnell, T. Tuma, B. Rajendran, Y. Leblebici, A. Sebastian, E. Eleftheriou, Neuromorphic computing with multi-memristive synapses, *Nat. Commun.* 9 (2018) 2514.
- [3] M.Y. Rao, H. Tang, J.B. Wu, W.H. Song, M.X. Zhang, W.B. Yin, Y. Zhuo, F. Kiani, B.J.M. Chen, X.Q. Jiang, H.F. Liu, H.Y. Chen, R. Midya, F. Ye, H. Jiang, Z. R. Wang, M.C. Wu, M. Hu, H. Wang, Q.F. Xia, N. Ge, J. Li, J.J. Yang, Thousands of conductance levels in memristors integrated on CMOS, *Nature* 615 (7954) (2023).
- [4] M.K. Song, J.H. Kang, X.Y. Zhang, W.J. Ji, A. Ascoli, I. Messaris, A.S. Demirkol, B.W. Dong, S. Aggarwal, W.E. Wan, S.M. Hong, S.G. Cardwell, I. Boybat, J.S. Seo, J.S. Lee, M. Lanza, H. Yeon, M. Onen, J. Li, B. Yildiz, J.A. del Alamo, S. Kim, S. Choi, G. Milano, C. Ricciardi, L. Alf, Y. Chai, Z.R. Wang, H. Bhaskaran, M. C. Hersam, D. Strukov, H.S.P. Wong, I. Valov, B. Gao, H.Q. Wu, R. Tetzlaff, A. Sebastian, W. Lu, L. Chua, J.J. Yang, J. Kim, Recent advances and future prospects for memristive materials, devices, and systems, *ACS Nano* 17 (13) (2023) 11994–12039.
- [5] F. Ghafoor, M. Ismail, H. Kim, M. Ali, S. Rehman, B. Ghafoor, M.A. Khan, H. Patil, S. Kim, M.F. Khan, D.K. Kim, Realization of future neuro-biological architecture in power efficient memristors of Fe₃O₄/WS₂ hybrid nanocomposites, *Nano Energy* 122 (2024) 109272.
- [6] B.K. Saika, R. Negishi, Y. Kobayashi, Neuromorphic switching behavior in multi-stacking composed of Pt/graphene oxide/Ag₂S/Ag, *Jpn. J. Appl. Phys.* 58 (1) (2019) 51D08.
- [7] H.Y.J. So, J.K. Lee, S. Kim, Short-term memory characteristics in n-type-ZnO/p-type-NiO heterojunction synaptic devices for reservoir computing, *Appl. Surf. Sci.* 625 (2023) 157153.
- [8] J. Sakhuja, S. Rowtu, S. Patil, S. Lashkare, U. Ganguly, Integration of non-filamentary Pr_{0.7}Ca_{0.3}MnO₃-based memristor with silicon-PN junction, *IEEE Electron. Device Lett.* 44 (5) (2023) 741–744.
- [9] Y. Zhang, S.H. Gao, G.M. Cao, C.R. Ma, H. Nan, M. Liu, Controllable resistive switching behaviors in heteroepitaxial LaNiO₃/Nb:SrTiO₃ Schottky junctions through oxygen vacancies engineering, *Nanotechnology* 34 (37) (2023) 375201.
- [10] L.Y. Shi, G.H. Zheng, B.B. Tian, B. Dkhil, C.G. Duan, "Research progress on solutions to the sneak path issue in memristor crossbar arrays," *Nanoscale Adv.* 2 (5) (2020) 1811–1827.

- [11] S.G. Ren, A.W. Dong, L. Yang, Y.B. Xue, J.C. Li, Y.J. Yu, H.J. Zhou, W.B. Zuo, Y. Li, W.M. Cheng, X.S. Miao, Self-rectifying memristors for three-dimensional in-memory computing, *Adv. Mater. (Early Access)* (2023) 36 (4) (2024) 2307218.
- [12] Y. Zhu, J.S. Liang, V. Mathayan, T. Nyberg, D. Primetzhofer, X. Shi, Z. Zhang, High performance full-inorganic flexible memristor with combined resistance-switching, *Acs Appl. Mater. Inter.* 14 (18) (2022) 21173–21180.
- [13] N.I. Mou, M. Tabib-Azar, Photoreduction of Ag⁺ in Ag/Ag₂S/Au memristor, *Appl. Surf. Sci.* 340 (2015) 138–142.
- [14] Y.X. Liu, L. Wu, Q. Liu, L. Liu, S.W. Ke, Z.H. Peng, T.Y. Shi, X.R. Yuan, H. Huang, J. Li, C. Ye, P.K. Chu, J.H. Wang, X.F. Yu, Topochemical synthesis of copper phosphide nanoribbons for flexible optoelectronic memristors, *Adv. Funct. Mater.* 32 (14) (2022) 2110900.
- [15] M.R. Chen, Y.F. Lv, X. Guo, X. Peng, J.H. Xi, L. Fu, S.C. Zhao, Investigation of resistive switching behaviors of cuprous phosphide thick film, *J. Alloys Compd.* 970 (2024) 172641.
- [16] X. Shi, H.Y. Chen, F. Hao, R.H. Liu, T. Wang, P.F. Qiu, U. Burkhardt, Y. Grin, L.D. Chen, Room-temperature ductile inorganic semiconductor, *Nat. Mater.* 17 (7) (2018) 421–426.
- [17] S. Jo, S. Cho, U.J. Yang, G.S. Hwang, S. Baek, S.H. Kim, S.H. Heo, J.Y. Kim, M.K. Choi, J.S. Son, Room-temperature ductile inorganic semiconductor, *Adv. Mater.* 33 (23) (2021) 2100066.
- [18] X. Peng, Y.F. Lv, L. Fu, F. Chen, W.T. Su, J.Z. Li, Q. Zhang, S.C. Zhao, Photoluminescence properties of cuprous phosphide prepared through phosphating copper with a native oxide layer, *RSC Adv.* 11 (54) (2021) 34095–34100.
- [19] Y. Zhu, J.S. Liang, V. Mathayan, T. Nyberg, D. Primetzhofer, X. Shi, Z. Zhang, High performance full-inorganic flexible memristor with combined resistance-switching, *Acs Appl Mater Inter* 14 (18) (2022) 21173–21180.
- [20] X. Peng, Y.F. Lv, J.H. Xi, L. Fu, F. Chen, W.T. Su, J.Z. Li, S.C. Zhao, Preparation and near-infrared photoelectric properties of n-type Cu₃P, *ChemistrySelect* 7 (43) (2022) e202202662.
- [21] M.M. Dong, Y.F. Lv, X. Peng, S.C. Zhao, Investigation of photoelectric behaviors of silver sulfide particles in different surroundings, *RSC Adv.* 12 (2) (2021) 1028–1034.
- [22] Y.Y. Yang, P. Gong, W.D. Ma, R. Hao, X.Y. Fang, Effects of substitution of group-V atoms for carbon or silicon atoms on optical properties of silicon carbide nanotubes, *Chin. Phys. B* 30 (6) (2021).
- [23] F. Yang, M.Y. Han, F.G. Chang, Zero temperature coefficient of resistivity induced by photovoltaic effect in YBa₂Cu₃O_{6.96} ceramics, *Aip Advances* 5 (1) (2015) 017126.
- [24] Z.H. Xu, L. Tang, S.W. Zhang, J.Z. Li, B.L. Liu, S.C. Zhao, C.J. Yu, G.D. Wei, 2D MoS₂/Cu₃P heterojunction based highly sensitive photodetectors through ultrafast charge transfer, *Materials Today Physics* 15 (2020) 100273.
- [25] M.M. Dong, Y.F. Lv, X. Peng, S.C. Zhao, Investigation of photoelectric behaviors of silver sulfide particles in different surroundings, *RSC Adv.* 12 (2021) 1028–1034.